

1.

U-Zr

U-Pu-Zr

가

가

[1,3].

가
가

LOCA

(fission production)
가

(solid swelling)
[1-5].

가

(swelling)

(cavity)

[6-8].

U Zr

Zr

billet

Zr-U/Zr-Nb

Zr-U

Zr-Nb

가 Zr-U

Zr-Nb

가

2.

U

derby

μm
 μm

Zr

125 μm
hydriding-dehydriding

Zr

U

Zr-40wt% U

가 45 μm

48
, 125

1500

2

Zr-U

Zr-1wt%Nb

590 700

4000

OM (optical microscope)

SEM (scanning electron microscope)

, EDS (Energy dispersive spectroscopy)

XRD (X-ray diffraction)

3.

3.1. Zr-U

1 Zr-U

Zr-U

$\delta\text{-UZr}_2$

$\alpha\text{-Zr}$

(Hv) 263

2 U-Zr

XRD pattern

$\alpha\text{-Zr}$ (hcp,

a=0.3232 nm, c=0.5147 nm)

$\delta\text{-UZr}_2$ (hcp, a=0.3080 nm, c=0.5030 nm)

U 가 U U

3 U-Zr [6]. 60
 wt% Zr 40wt%U
 10% δ -UZr₂ 90% α -Zr , α -Zr
 (γ -U, β -Zr)
 606 γ -U β -Zr δ -UZr₂
 α -Zr 가 (2).

3.2. Zr-Nb

4 Zr-Nb rod Zr-Nb
 extrusion Zr-Nb rod
 (Hv) 155
 5 Zr-Nb XRD α -Zr (hcp, α -
 a=0.3232 nm, c=0.5147 nm)
 pilgering 650 , 580 2 annealing
 6 Zr-Nb Zr-1Nb 가 α -Zr β -
 610-860 α -Zr β -Zr , 610 Nb

3.3. Zr-U/ZrNb

7 Zr-U/ZrNb Zr-
 Nb Zr-U pore
 α -Zr

3.4.

8 590 가 가
 Zr-U α -Zr 가
 가 α -Zr 가
 9 700 4000 [10-11].
 700 700 α -Zr dissolution
 700 α -Zr δ -UZr₂ U-Zr (3) 가
 (γ -U, β -Zr)
 10 590

700 Zr-U 가 500

500

11 590 700 4000 Zr-U XRD pattern (α-Zr β-Zr (cubic, a = 0.3545 nm) (3). α δ β-Zr (β-Zr) 가 , 700 4000 α δ β-Zr (β-Zr) 가 4000

3.5. 가 12 590 가 가 1500 13 700 가 Zr-Nb 가 가

14 590 700 가 Zr-Nb 가 590 가 700 500 가 700 500 가

15 590 700 Zr-Nb XRD pattern (15a), 590 Zr-Nb 가 β-Zr (cubic, a=0.3545 nm) β-Zr 700

3.6. Zr-U/Zr-Nb 16 590 4000 Zr-U/Zr-Nb 가 U 가 Zr-Nb 가 590

17 700 4000 Zr-U 가 가 590 700 700 Zr, U 가 가 590

18 590 700 4000 가 가 590 700 가 가

Zr, U

가 (D) (x² = 2 D t) 가

[12]. Zr-U/Zr-Nb (D) 500 700°C

1.1-1.6×10⁻¹⁵ 4.0-4.5×10⁻¹⁵ m²/s

4.

Zr-U Zr-Nb

Zr-40U 590°C

가 α-Zr δ-UZr₂ β-Zr 가 700°C

Zr-U 590°C Zr-1Nb

β-Zr 700°C

700°C 가 Zr-U/Zr-Nb (D) 500

1.1-1.6×10⁻¹⁵ 4.0-4.5×10⁻¹⁵ m²/s

1. G.L.Hofman, L.C.Walters and T.H.Bauer, *Progress in Nuclear Energy*, 31, No.1/2, pp. 83-110, 1997.
2. T. Ogata, M. Kurata, K. Nakamura, A. Itoh and M. Akabori, "Reaction between U-Zr alloys and Fe at 923K" *J. Necl. Mater.* 250, pp. 171-175, 1997.
2. C.E. Till, I. Chang Y. and W.H. Hannum, *Prog. in Nucl. Energy*, 31, pp. 3-11, 1997.
3. D.D. Keiser, Jr. and M.A. Dayananda, *Metallurgical Transaction A*, 25A, pp. 1649, 1994.
4. G.L. Hofman, L.C. Walters and T.H. Bauer, *Prog. in Nucl. Energy*, 31, pp. 83-110, 1997.
5. Nikishov O.A., et al. "U-Zr metal fuel" Private comunication.
6. H.Okamoto, *Journal of Phase Equilibria*, 13(1), 1992.
7. A.D. Smigelskas and E.O. Kirkendal, *Trans. Met. Soc. AIME*, 171:130, 1947.
8. D.A. Porter and K.E. Easterling, *Phase Transformation in Materials*, 2nd Ed. 1992.
9. M. Akabori, A. Itoh, T. Ogawa and T. Ogata, "Interdiffusion in the U-Zr system at δ-phase compositions" *J. Alloys Comp.* Vol. 271-273, pp. 597-601, 1998.
10. , , , , , , 2003
11. , , , , , , 2003
12. M.Akbori, A.Itoh, T.Ogawa, T.Ogata, *J. Alloy. Comp.*, 271, pp. 597-601, 1998.

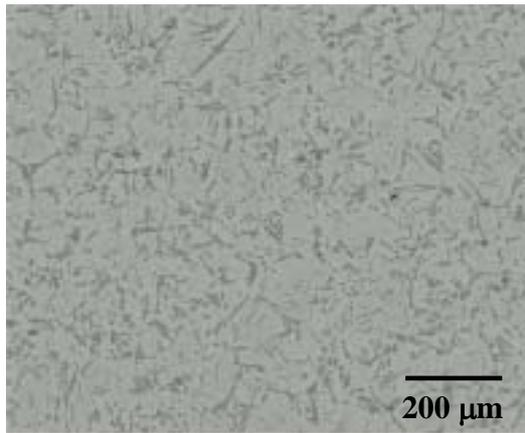


Fig. 1. Microstructure of sintered Zr-U alloy.

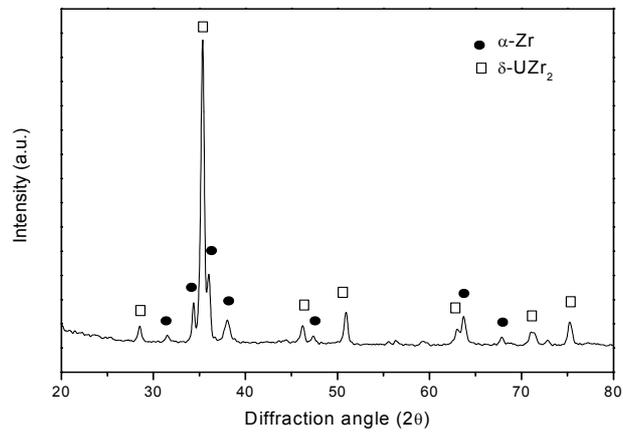


Fig. 2. X-ray diffraction pattern on the sintered U-Zr alloy.

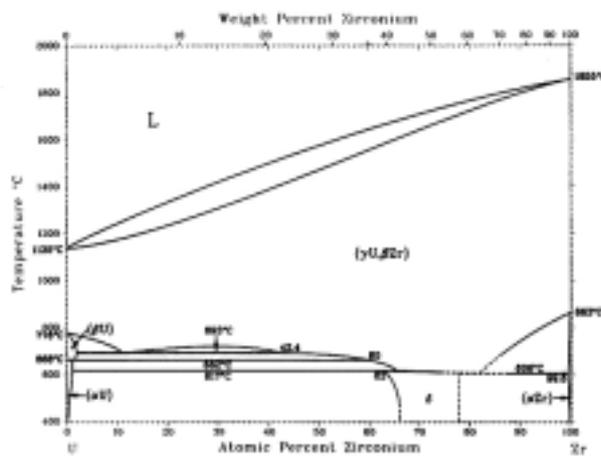


Fig. 3. Equilibrium phase diagram of Zr-U binary system [6].

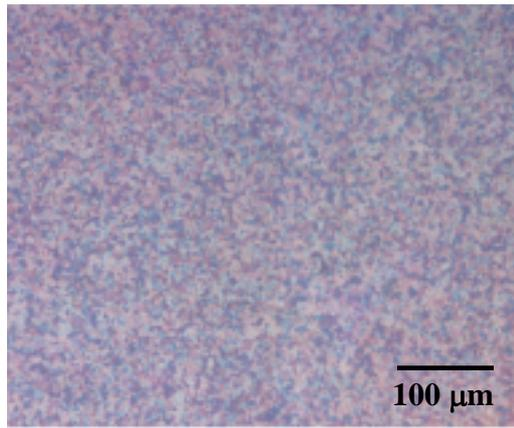


Fig. 4. Microstructure of Zr-Nb alloy.

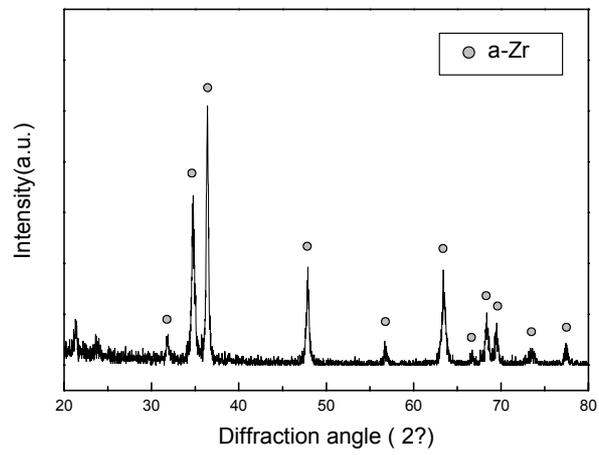


Fig. 5. X-ray diffraction pattern on the Zr-Nb alloy.

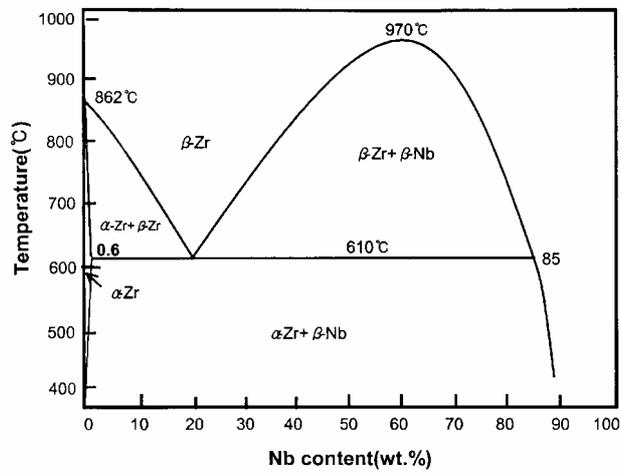


Fig. 6. Equilibrium phase diagram of Zr-Nb binary system.

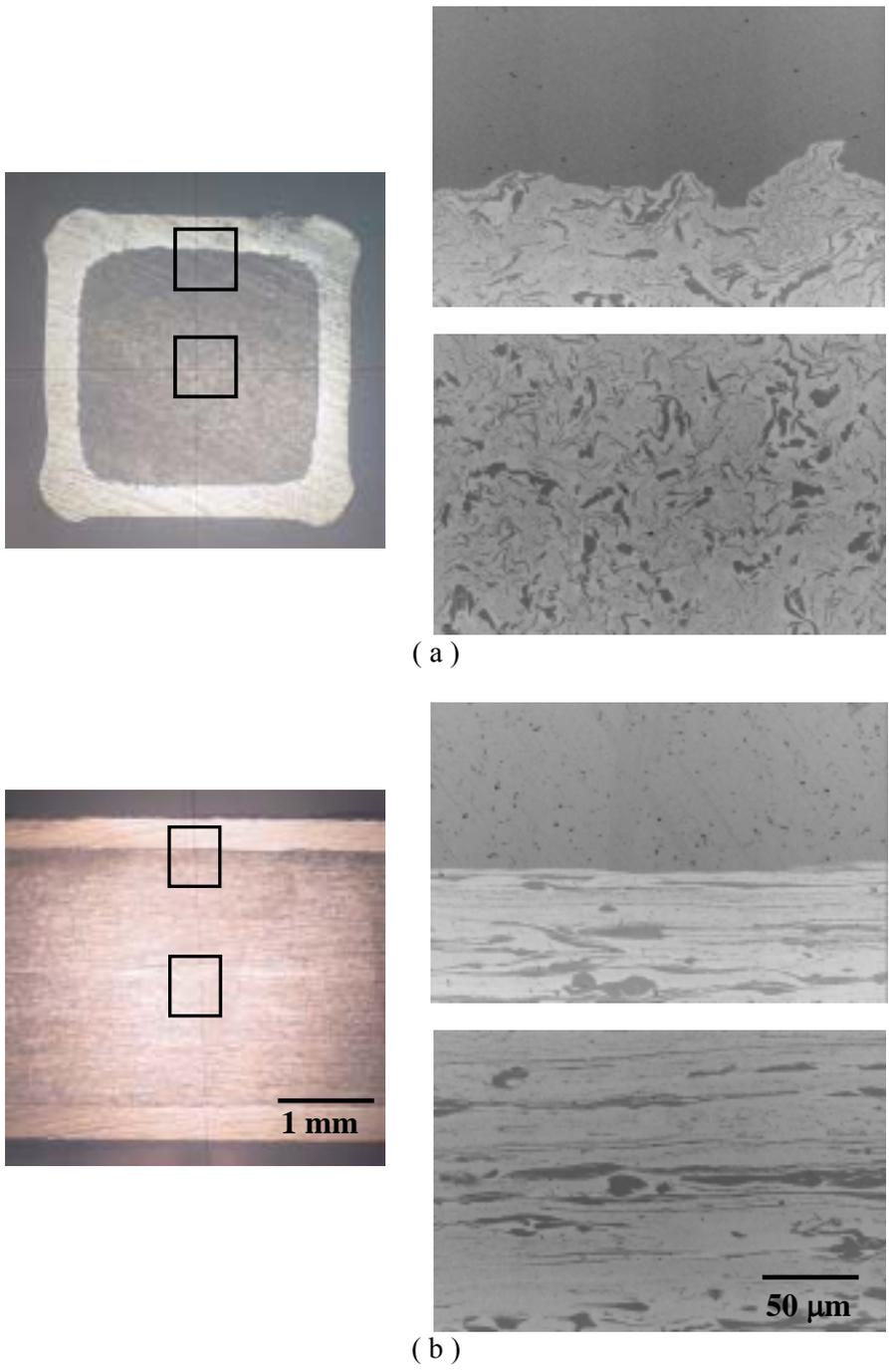


Fig. 7. Microstructures of Zr-U/Zr-Nb extruded rods; (a) transverse and (b) longitudinal sections.

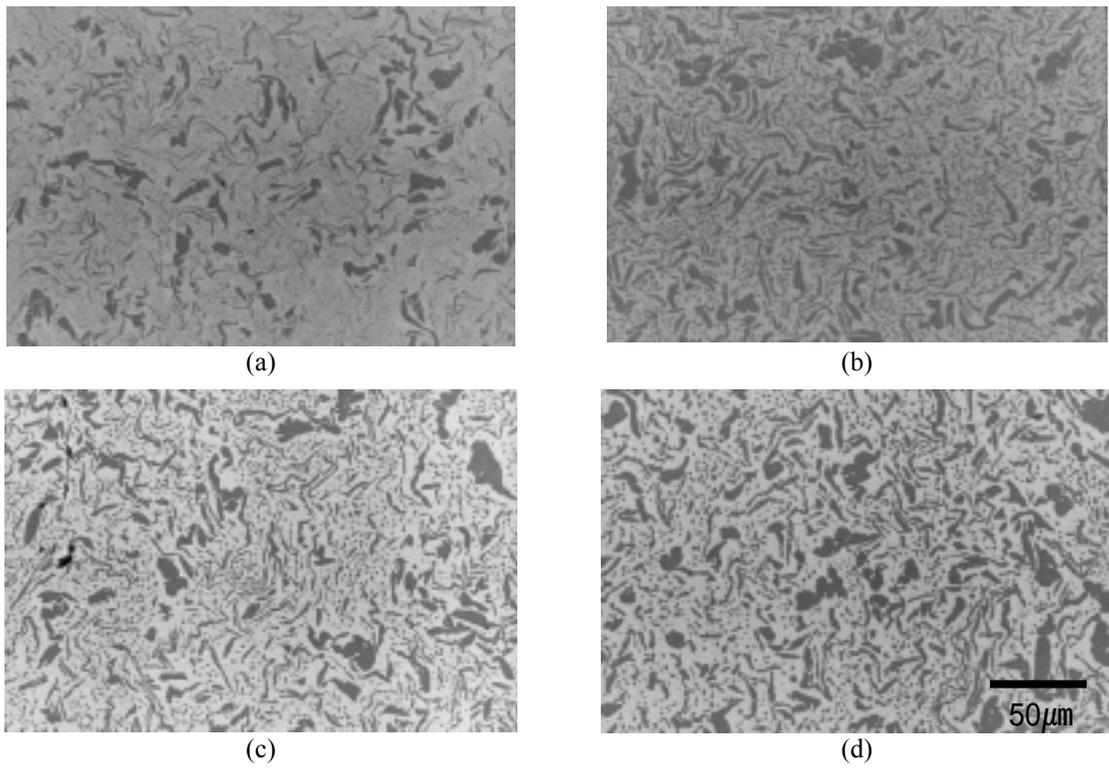


Fig. 8. SEM-BEI images of Zr-U fuel after heat-treatment at 590 °C for (a) 0, (b) 1000, (c) 2000 and (d) 4000 hours.

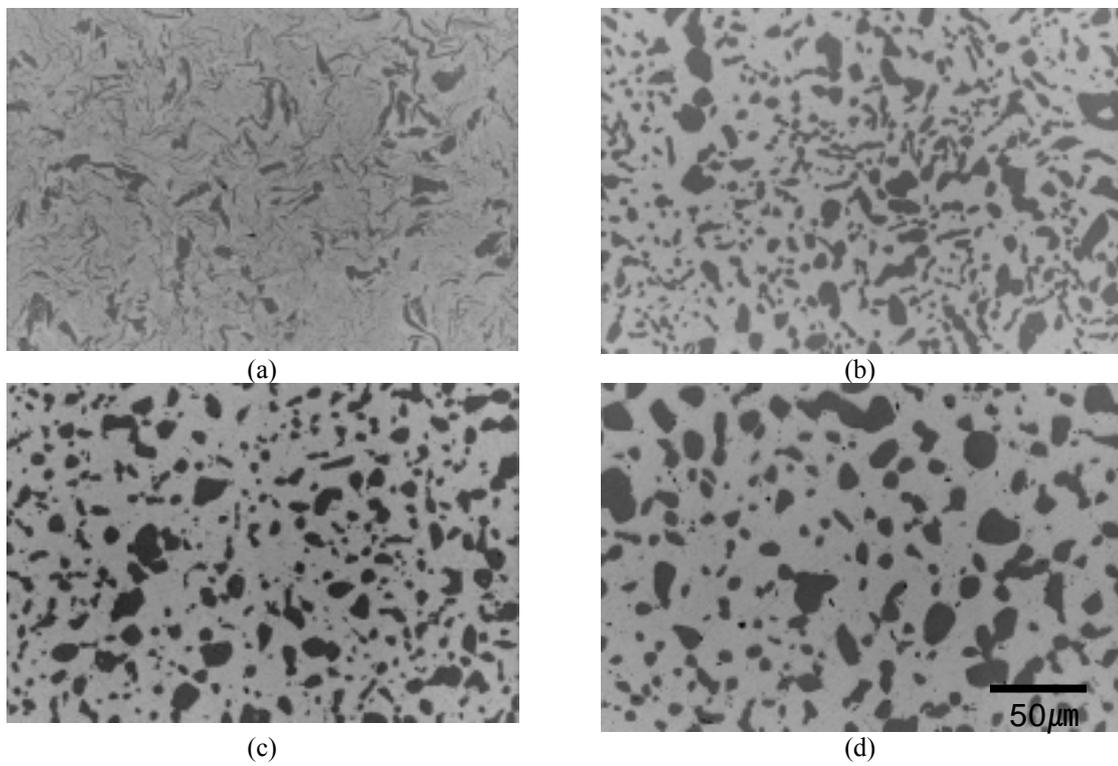


Fig. 9. SEM-BEI images of Zr-U fuel after heat-treatment at 700 °C for (a) 0, (b) 500, (c) 1000, (d) 1500, (e) 2000 and (f) 4000 hours.

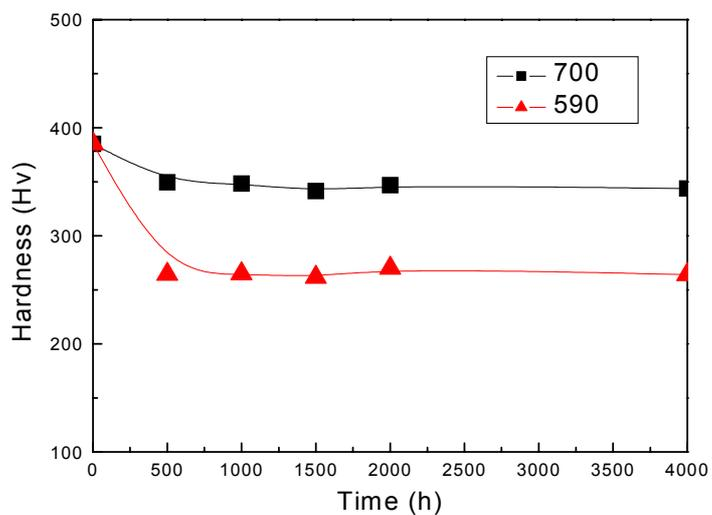


Fig. 10. Effects of heat-treatment on the hardness of Zr-U fuel in Zr-U/Zr-Nb extruded rod.

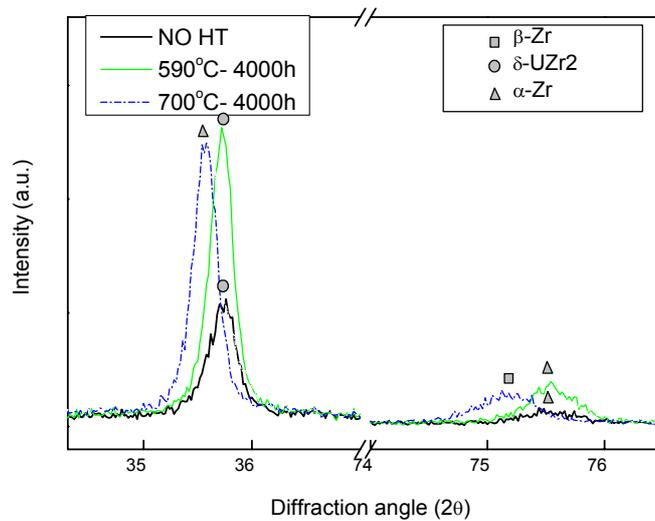


Fig. 11. X-ray diffraction patterns of Zr-U alloy after heat-treatment at 590 and 700 for 4000 hours.

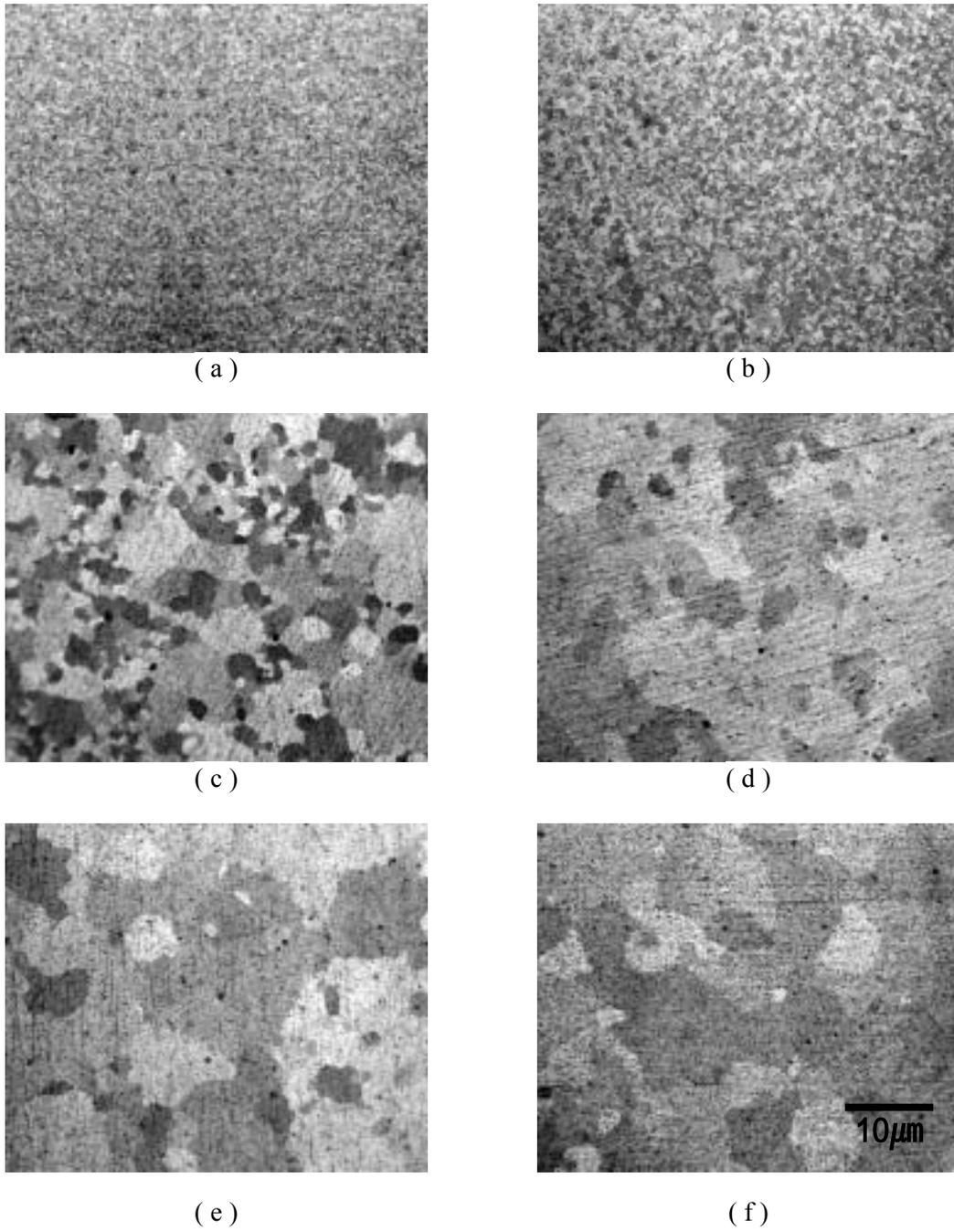


Fig. 12. Microstructures of Zr-Nb cladding after heat-treatment at 590 °C for (a) 0, (b) 500, (c) 1000, (d) 1500, (e) 2000 and (f) 4000 hours.

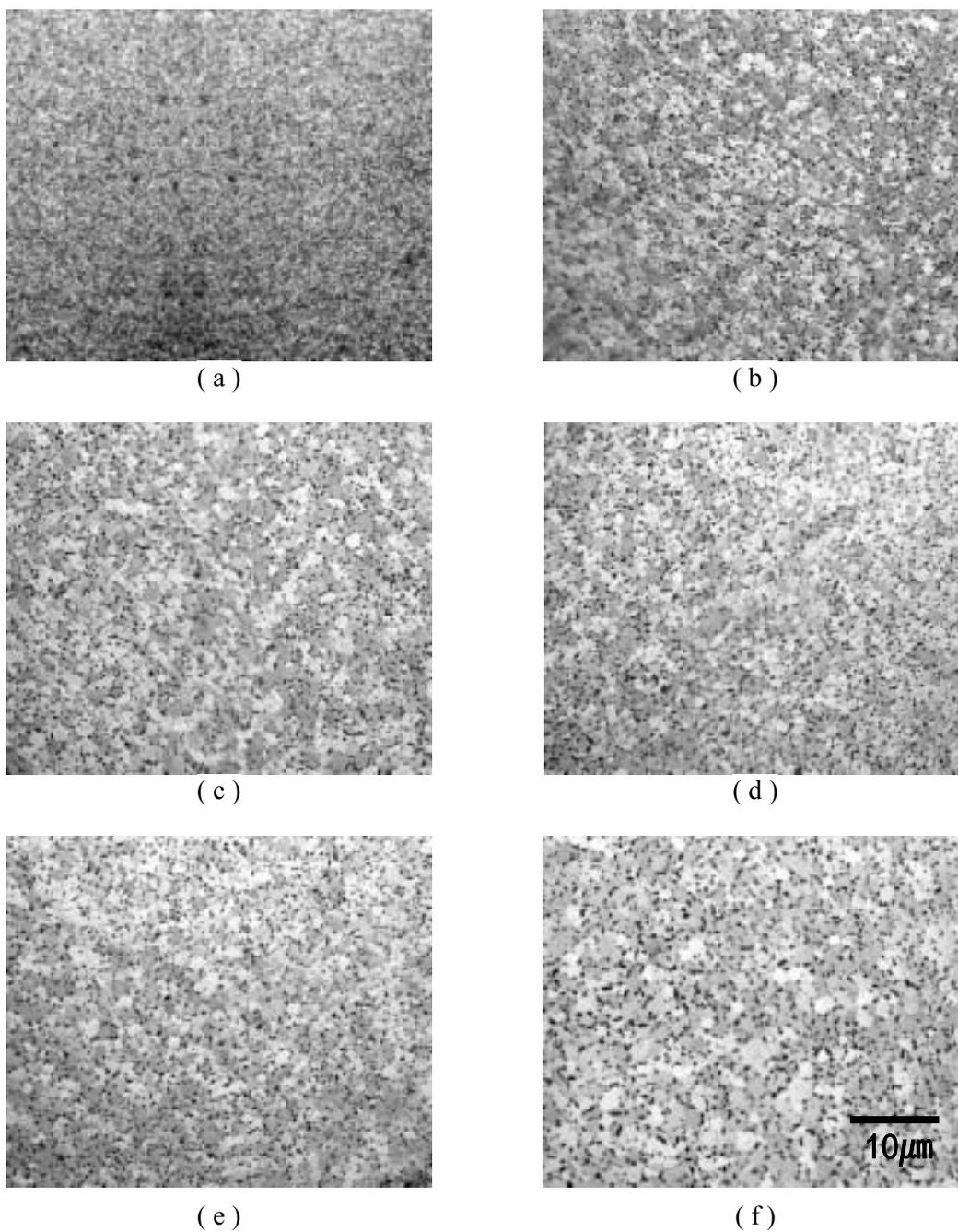


Fig. 13. Microstructures of Zr-Nb cladding after heat-treatment at 700 °C for (a) 0, (b) 500, (c) 1000, (d) 1500, (e) 2000 and (f) 4000 hours.

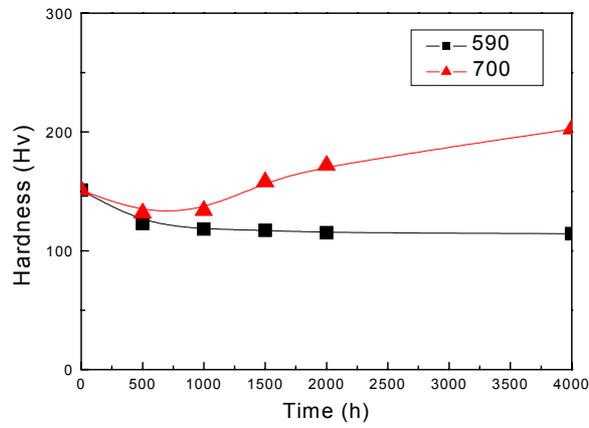
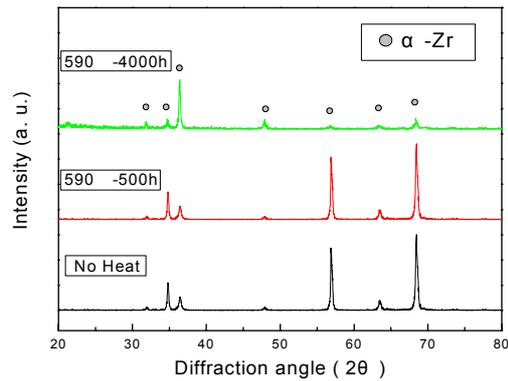
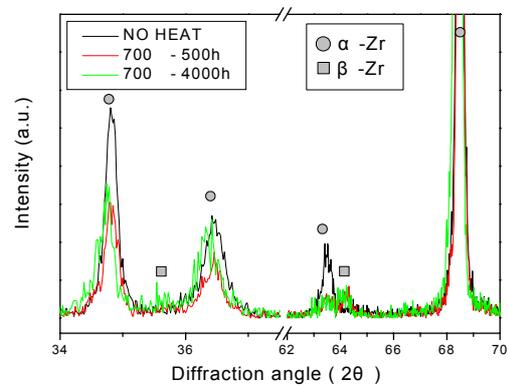


Fig. 14. Effects of heat-treatment on the hardness of Zr-Nb cladding in Zr-U/Zr-Nb extruded rod.



(a)



(b)

Fig. 15. X-ray diffraction patterns of Zr-Nb cladding after heat-treatment at (a) 590 and (b) 700 .

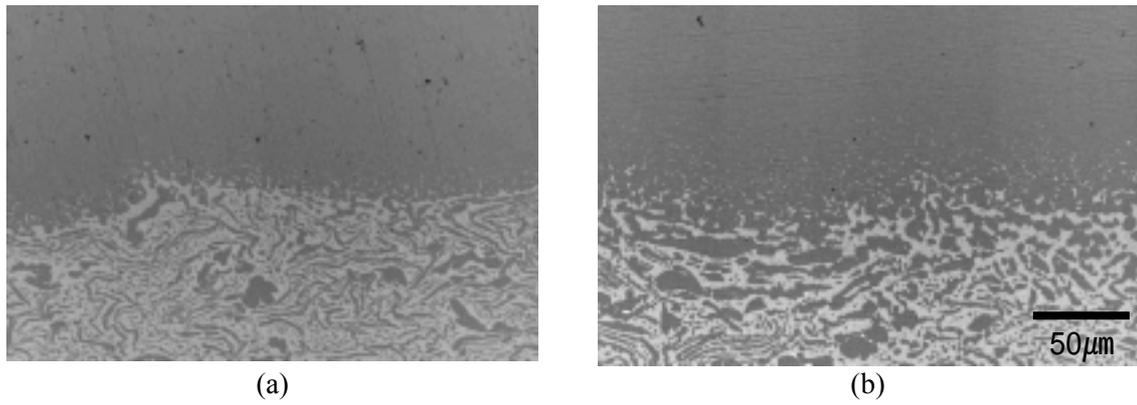


Fig. 16. SEM-BEI images of Zr-U/Zr-Nb interface after heat-treatment at 590 °C for (a) 2000 and (b) 4000 hours.

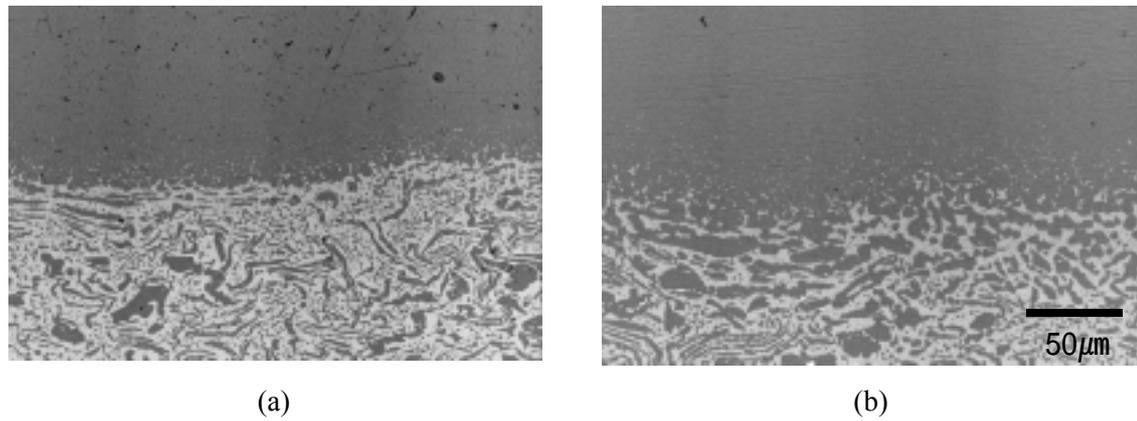


Fig. 17. SEM-BEI images of Zr-U/Zr-Nb interface after heat-treatment at 700 °C for (a) 2000 and (b) 4000 hours.

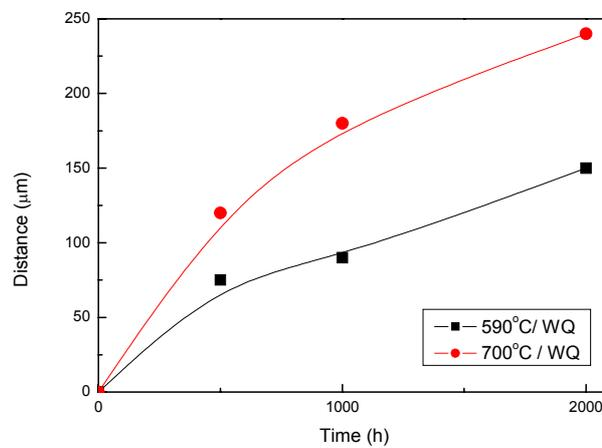


Fig. 17. Variation of thickness of reaction layer in Zr-U/Zr-Nb interface with time.